ELSEVIER

International Journal of Minerals, Metallurgy and Materials
Volume 16, Number 6, December 2009, Page 661

Materials

Effect of Ca^{2+} on CO_2 corrosion properties of X65 pipeline steel

Chen Ding[1)], *Ke-wei Gao*[1)], *and Chang-feng Chen*[2)]

1) Department of Materials Physics and Chemistry, University of Science and Technology Beijing, Beijing 100083, China
2) Department of Materials, China University of Petroleum, Beijing 100083, China
(Received 2008-12-10)

Abstract: The effect of Ca^{2+} on CO_2 corrosion to X65 pipeline steel was investigated in the simulated stratum water of an oil field containing different concentrations of Ca^{2+}. It is found that Ca^{2+} can enhance the corrosion rate, especially in the Ca^{2+} concentration from 256 to 512 mg/L, which can be attributed to the growing grain size and loosing structure of corrosion scales with increasing Ca^{2+} concentration. X-ray diffraction (XRD) and X-ray photoelectron spectroscopy (XPS) investigations reveal that a complex carbonate (Fe, Ca)CO_3 forms at high Ca^{2+} concentration due to the gradual replacement of Fe^{2+} in $FeCO_3$ by Ca^{2+}.

Key words: CO_2 corrosion; pipeline steel; stratum water; Ca^{2+} concentration; complex carbonate

[*This work was financially supported by the National Natural Science Foundation of China (No.50571012).*]

1. Introduction

In oil and gas fields, the stratum water often contains many mineral ions such as Ca^{2+} and Mg^{2+}, which lead to a precipitation of scales and may influence the susceptibility to uniform corrosion during CO_2 corrosion. For example, severe CO_2 corrosion of oil tubes was reported in the Shengli Oil Field in China where the stratum water was rich in calcium (15 g/L) [1]. Although many studies in the laboratory [2-3] have been carried out to simulate the CO_2 corrosion behavior of pipeline steel in simulated solutions, few works focused on corrosion problems of carbon steel in the solution of rich Ca^{2+} [4].

Sun [5] investigated the effect of Ca^{2+} on pitting morphology in CO_2 environment. The results indicated that in the solution without any metallic cations, the P110 steel presented typical V-shape pitting, whereas in the solution containing Ca^{2+}, the V-shape together with semi-spherical and closed spherical pitting appeared. Jiang [6] researched on the effect of Ca^{2+} on the pitting corrosion and inhibition performance in CO_2 corrosion of N80 steel and considered that under static and the same Cl^- concentration, adding Ca^{2+} did not change the optimum inhibitor concentration.

Above all, Ca^{2+} plays an important role in CO_2 corrosion and it is necessary to understand the effect of Ca^{2+} on corrosion properties such as morphology of corrosion scales, composition and mechanical properties, so the structure and mechanical properties were detailed studied in the present work.

2. Experimental

All experiments were carried out under static conditions at 75°C and 1 MPa CO_2 partial pressure for 10 d in a simulated solution of stratum water in an oil field. The chemical composition of the solution is shown in Table 1. Ca^{2+} concentration in the simulated solution was set up at 64, 128, 256, and 512 mg/L as Zhang did [7]. Although Ca^{2+} was added to the solution as $CaCl_2$, there was a lot of Cl^- existed as NaCl and the effect of Cl^- in $CaCl_2$ could be ignored. The experimental material was API-X65 pipeline steel. Its chemical composition is shown in Table 2. The specimen dimension was 1 cm×1 cm×1 mm and the surface of specimens was polished with silicon carbide paper up to 800-grit, rinsed with distilled water and degreased with acetone.

Cambridge S360 Scanning Electron Microscope (SEM) was used to observe the surface and cross-sec-

Corresponding author: Ke-wei Gao, **E-mail:** kwgao@yahoo.com
Also available online at www.sciencedirect.com

cross-section morphologies of CO_2 corrosion scales. League 2000 Energy Dispersive Spectrometer (EDS) was used to analyze the composition and the distribution of Ca^{2+} in the scales. X-ray Diffraction (XRD) and X-ray Photoelectron Spectroscopy (XPS) analysis were carried out to determine the microstructure of the scales and the quantivalence of each element in the corrosion scales.

Table 1. Ion concentration in the simulated solution **mg·L^{-1}**

Na^++K^+	Ca^{2+}	Mg^{2+}	Cl^-	SO_4^{2-}	HCO_3^-	CO_3^{2-}	Total
2568	64/128/256/512	78	3580	48	863	153	7354/7418/7546/7802

Table 2. Chemical composition of the testing materials **wt%**

C	Si	Mn	Mo	Fe
0.04	0.2	1.5	0.02	balance

3. Results and discussion

3.1. Corrosion rate and morphology of corrosion scales

Fig. 1 illustrates the corrosion rate under different Ca^{2+} concentrations. It indicates that the corrosion rate of X65 steel increases with increasing Ca^{2+} concentration. The corrosion behavior of Ca^{2+} with different concentrations can be explained as the following: firstly, Ca^{2+} increases the pH value of the solution which causes the increase of the Henry's constant of CO_2 in the solution, in some extent, the higher the Ca^{2+} concentration, the lower the CO_2 solubility is in the solution; secondly, Ca^{2+} can change the formation of the corrosion scales and accelerate under-scale corrosion and galvanic corrosion between the corrosion scales and matrix. These two reasons lead to a high uniform corrosion rate.

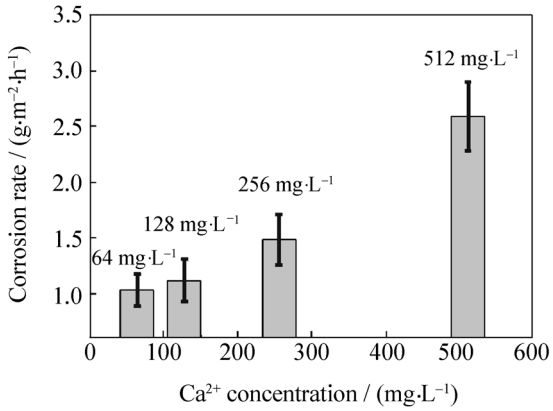

Fig. 1. Corrosion rate of X65 pipeline steel under different Ca^{2+} concentrations.

Fig. 2 shows SEM observations of the surface corrosion scales. With the increase of Ca^{2+} concentration the corrosion scales become looser and the grain size gets bigger, which will cause the strength and adhesive force of the scales to matrix decrease. Under high Ca^{2+} concentration, liquid flow will make the corrosion scales delaminate easily. These loose corrosion scales can not stop corrosive ions diffusing through the scales effectively which may lead to a high corrosion rate.

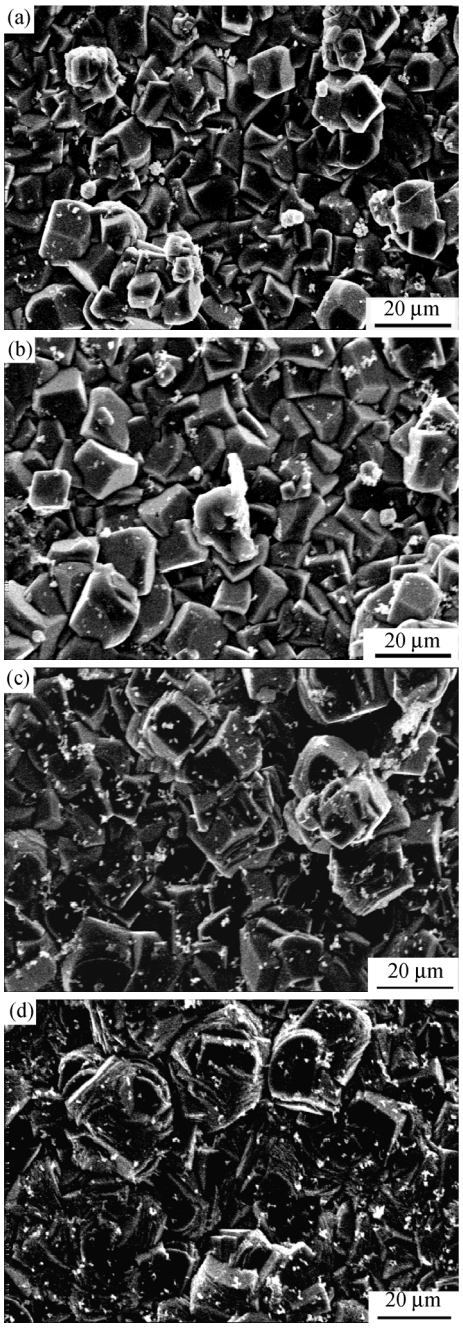

Fig. 2. Surface SEM images of corrosion scales under different Ca^{2+} concentrations: (a) 64 mg/L; (b) 128 mg/L; (c) 256 mg/L; (d) 512 mg/L.

3.2. XRD analysis of CO_2 corrosion scales

From Fig. 3 it can be concluded that most of the scales are composed by $FeCO_3$. According to Lin, Fe_3C, Fe_2O_3 should be detected in the corrosion scales [8], but there are no obvious Fe_3C and Fe_2O_3 peaks in Fig. 3(a). The reason is that the surface corrosion scales are relatively thick under high pressure CO_2 conditions [9]. After being taken out of the autoclave, the specimens were not exposed to air for a long time which may lead to decomposition of $FeCO_3$. Besides, with the increase of Ca^{2+} concentration, almost all of the diffraction peaks of $FeCO_3$ move to a lower diffraction angle, which can be observed more obviously in Fig. 3(b), and the moving distance has a good agreement with the proportion of Ca^{2+} concentration, which indicates that the compounds of calcium became more and more in the corrosion scales [10]. The reason for this is that $FeCO_3$ and $CaCO_3$ have the same chemical formula and crystal structure, and the Fe and Ca ionic radius are also very close to each other, therefore, these two compounds can exchange the corresponding elements without changing their crystal structures, and this phenomenon is called isomorphism [11]. Fe^{2+} can be replaced by Ca^{2+} in the $FeCO_3$ crystal structure, and (Fe, Ca)CO_3 forms which is called complex carbonate [1]. In complex carbonate, the type of chemical bonds and the balance of ionic positive and negative charges are constant, and the cell parameters and physical property (refractive index, specific weight, *etc.*) appear lineal variation with substitution quantity [10,12]. The lattice constants of a, b, and c (a=b) become much bigger after atoms replacing because the radius of Ca atoms (0.197 nm) is longer than that of Fe (0.127 nm). According to the Bragg equation:

$$2d\sin\theta=n\lambda$$

where d is the spacing between the planes in the atomic lattice, θ the angle between the incident ray and the scattering planes, n an integer determined by the order given, λ the wavelength of the incident wave.

When the interplanar distance increases, the diffraction angle reduces and the corresponding XRD peaks move to low angles.

3.3. EDS analysis of CO_2 corrosion scales

Fig. 4 shows the line scanning energy spectrum of calcium in the corrosion scales under the conditions of 1 MPa CO_2 partial pressure and 128 mg/L of Ca^{2+} concentration. It can be seen that the amount of calcium in the corrosion scales is higher than that in matrix; further more, it is also higher in the surface scale than in the inner scale.

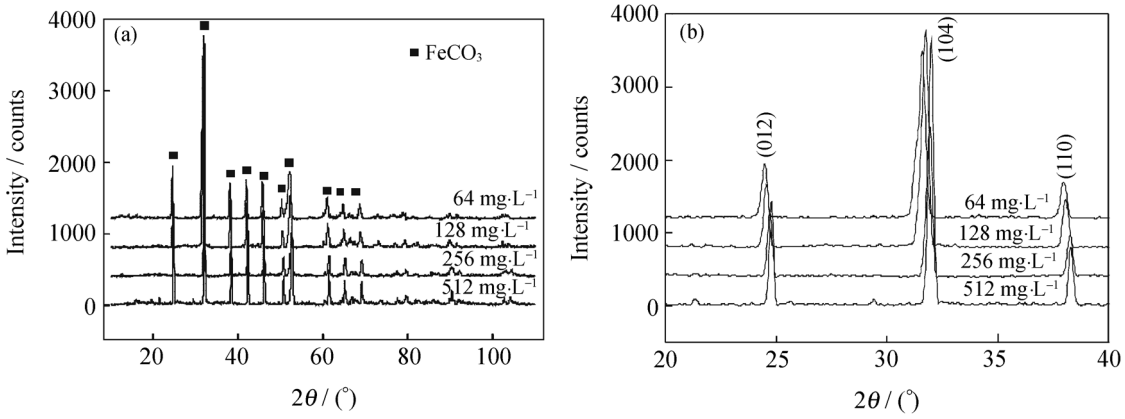

Fig. 3. XRD pattern of corrosion scales under different Ca^{2+} concentrations (a) and its partial high magnification image (b).

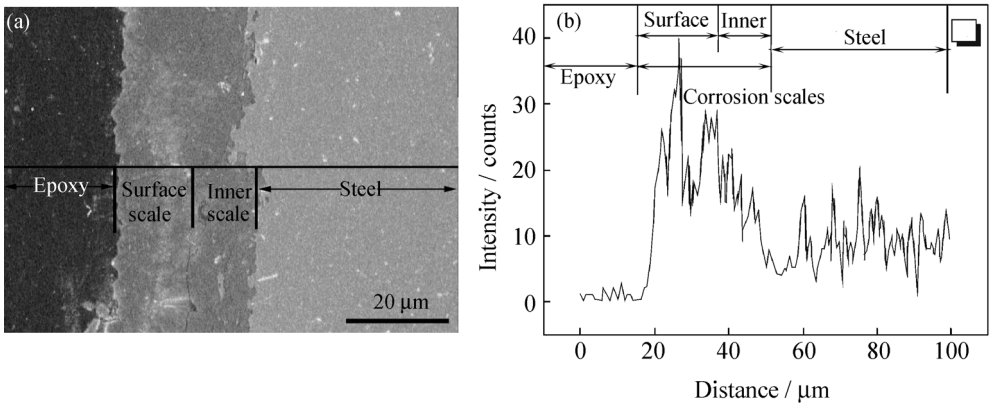

Fig. 4. EDS analysis of Ca on the cross-section of the corrosion scales.

Fig. 5 shows that the Ca^{2+} content is higher in the surface scale than the inner scale, and the atomic ratio of Ca/Fe also increases with increasing Ca^{2+} concentration, which indicates Ca^{2+} accumulating in the corrosion scales, especially in the surface scale. When the value of $[Fe^{2+}]\times[CO_3^{2-}]$ in the corrosion solution surpasses the solubility product constant of $FeCO_3$, $FeCO_3$ deposits on the specimen surface. Ca^{2+} diffusion begins on the surface scale, and there should be a differential concentration between the surface and inner scale, so calcium has a high level of content in the surface scale [8, 10]. It indicates that most replacements between Ca^{2+} and Fe^{2+} happen after $FeCO_3$ formed. According to the study of Palacios and Shadley [3], the inner scale was porous and formed before the surface scale. Comparing with the inner scale, the surface scale is more compacted. It can be seen that the surface layer of the corrosion scales had higher concentrations of Ca and Sarin found the same characteristic of silicon [13].

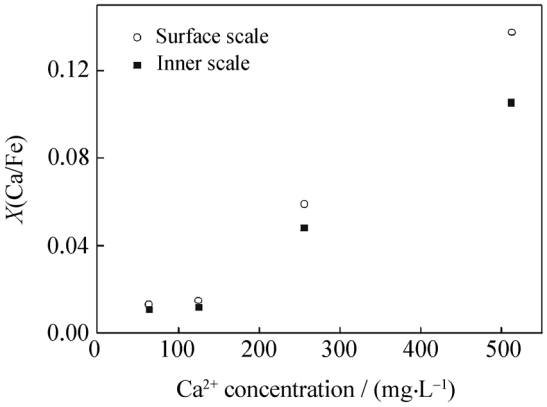

Fig. 5. Comparison of the atomic ratio of Ca/Fe in the surface and inner corrosion scales

3.4. XPS analysis

An examination of Fe2p, Ca2p, C1s and O1s peaks under different Ca^{2+} concentration conditions is shown in Fig. 6. The scan of the C1s binding energy under the 64 mg/L Ca^{2+} concentration condition reveals two peaks that the one is 288.93 eV corresponding to carbonate, and the other is 284.54 eV corresponding to the adventitious hydrocarbons adsorbed on all specimens. The binding energies of the compounds from the literature have been corrected by C1s peak values and the standard binding energies for elements are reported in Table 3.

Fig. 6(a) shows the fitting curve of binding energy spectrums of Fe element, it can be seen that the peak around 710.1 eV is $FeCO_3$. With the increase of Ca^{2+} concentration, the $Fe2p_{3/2}$ peak moved from 710.35 to 709.77 eV. XRD analysis has already shown that Ca^{2+} probably replaces Fe^{2+} during the forming of $FeCO_3$, and this may also lead to the change of binding energy of Fe. The shape of all the curves does not have any obvious change except slight shift. Comparing with the standard binding energy of $FeCO_3$ (Table 3), the change of binding energy under the highest Ca^{2+} concentration condition (512 mg/L) is 1.05 eV. In this case, the main chemical valence of iron in the corrosion scales is still ferrous (Fe^{2+}). It demonstrates that (Fe, Ca)CO_3 is stable in the corrosion scales, which agrees with XRD analysis and XPS results well in Fig. 6(a).

The fitting curve of calcium is shown in Fig. 6(b). When the Ca^{2+} concentration increases, the $Ca2p_{3/2}$ peak moved from 346.42 to 347.11 eV, from which it can be concluded that the chemical valence of calcium is stable in the corrosion scales and the intensity is a little higher under the 512 mg/L Ca^{2+} concentration condition than that in lower Ca^{2+} concentration conditions. According to the standard data, there may be Ca, CaS, $CaCO_3$, $CaSiO_4$, and $CaMnO_4$ in the corrosion scales. $CaCO_3$ is the most probable compound because it agrees with the standard data well. However, there are not any peaks of these compounds in XRD analysis despite of a large amount of Ca in EDS analysis. In addition, elements like Si and Mn are definitely not possible in this experiment. Given this, Ca is considered as part of complex carbonate (Fe, Ca) CO_3.

From Fig. 6(c) it can be seen that the C1s peak around 284.59 and 288.79 eV are related with the organic compound during the surface air adsorption and washing period and it does not have direct relations with the composition of the corrosion scales. The C1s peak around 288.93 eV corresponds to CO_3^{2-}, which indicates the surface scales is mainly formatted by carbonate and this peak can supply the information of carbonate [10]. When the Ca^{2+} concentration increases, the C1s peak associated with $FeCO_3$ drops significantly. However, the C1s peak does not obviously shift, which means the Ca^{2+} concentration can not change the fact that the main composition of the corrosion scales is carbonate. The results that the C1s peak does not obviously shift but its intensity decreases indicate that the main composition of the scales are still carbonate with increasing Ca^{2+} concentration, however the amount of carbonate in the scales decreases.

Fig. 6(d) shows the fitting curve of oxygen. It can be seen that the O1s peak is made up by 2 different peaks. The peak around 529.50 eV is associated with oxides and around 531.4 eV corresponds to carbonate in the corrosion scales [14].

With the increase of Ca^{2+} concentration, the peak

related with carbonate does not obviously change, however, the peak presenting oxide has a shift towards a lower binding energy, which is especially obvious under the 512 mg/L Ca^{2+} concentration condition. This indicates that in the corrosion scales, carbonate is still the main composition but the oxidation of the corrosion scales takes place more seriously under higher Ca^{2+} concentration conditions.

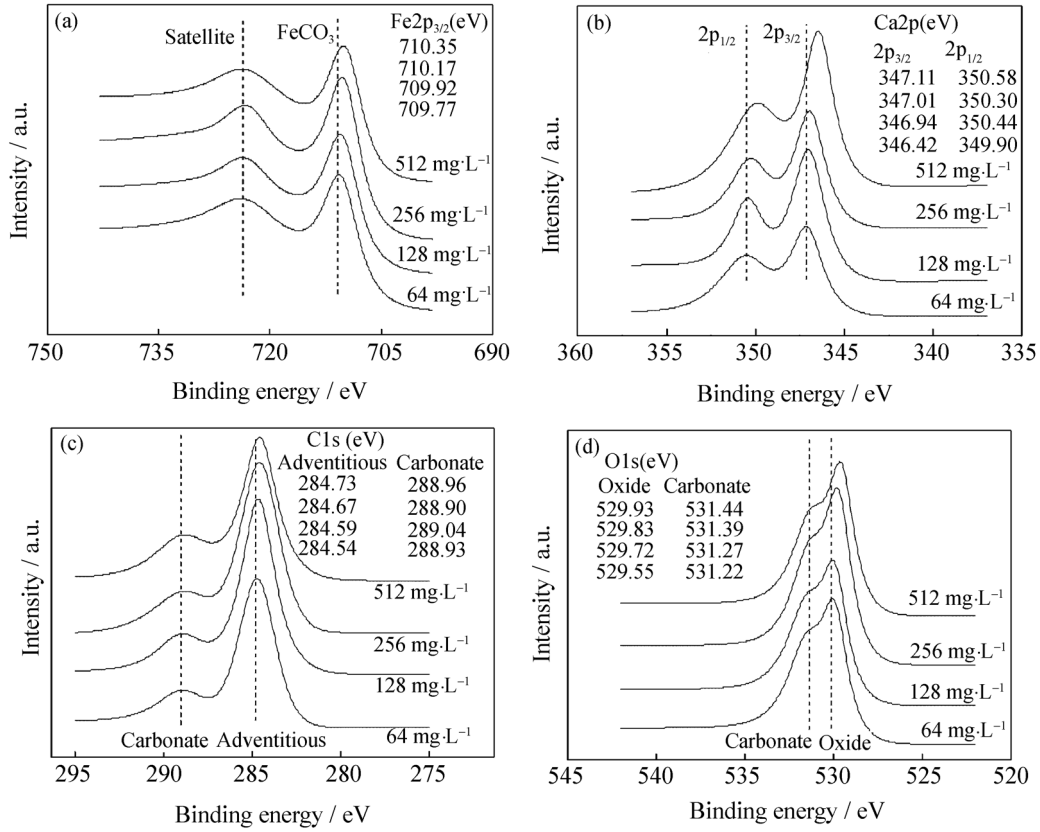

Fig. 6. Fitting peaks of Fe2p (a), Ca2p (b), C1s (c) and O1s (d) binding energies.

From the above analysis, it is concluded that the main composition of the corrosion scales includes carbonate and a small amount of iron oxidation. When the Ca^{2+} concentration increases, Fe^{2+} in $FeCO_3$ is replaced by Ca^{2+}, in this case, the binding energies of calcium, oxygen and carbon actually have some changes. These changes have given a support to the forming of (Fe, Ca) CO_3 when the Ca^{2+} concentration increases.

Table 3. Standard binding energy and speciation of elements analyzed by XPS

Element	Energy level	Binding energy / eV	Peaks
C	1s	284.6	Adventitious
		288.9	CO_3^{2-}
O	1s	529.5	O^{2-}
		531.0	CO_3^{2-} / OH^-
Fe	$2p_{3/2}$	709.3	$FeCO_3$
		713.9	Satellite
Ca	$2p_{3/2}$	346.6	$(Fe,Ca)CO_3$
		350.0	$(Fe,Ca)CO_3$

4. Conclusions

(1) Under static condition, the CO_2 corrosion rate in the simulated solution increases with increasing Ca^{2+} concentration from 64 to 512 mg/L.

(2) The grain size of the corrosion scales increases and the stack of grains become loose at higher Ca^{2+} concentrations, therefore the corrosion scales formatted under high Ca^{2+} concentration conditions can not suppress corrosive ions diffusing through the corrosion scales effectively.

(3) Ca^{2+} can gradually replace Fe^{2+} in $FeCO_3$ and forms complex carbonate $(Fe, Ca)CO_3$ with increasing Ca^{2+} concentration. $(Fe, Ca)CO_3$ is the only one calcium compound in the corrosion scales.

References

[1] S.L. Wu, Z.D. Cui, F. He, Z.Q. Bai, S.L. Zhu, and X.J. Yang, Characterization of the surface film formed from carbon dioxide corrosion on N80 steel, *Mater. Lett.*, 58(2004), p.1076.

[2] X.Y. Zhang, F.P. Wang, Y.F. He, and Y. L. Du, Study of the inhibition mechanism of imidazoline amide on CO_2 corrosion of Armco iron, *Corros. Sci*., 43(2001), No.8, p.1417.

[3] C.A. Palacios and J.R. Shadley, Characteristics of corrosion scales on steels in CO_2-saturated NaCl brine, *Corro-*

sion, 47(1991), No.2, p.122.

[4] Z.Xia, K.C. Chou, and Z. Szklarska-Smialowska, Pitting corrosion of carbon steel in CO_2-containing NaCl brine, *Corrosion*, 45(1989), No.8, p.636.

[5] D.B. Sun, J. Li, H.Y. Yu, M.X. Lu, M.L. Yan, and G.X. Zhao, Effect of Ca^{2+} and Mg^{2+} on pitting morphology in CO_2 environment, *J. Iron Steel Res.* (in Chinese), 13(2001), No.3, p.53.

[6] X. Jiang, Y.G. Zheng, D.R. Qu, and W. Ke, Effect of calcium ions on pitting corrosion and inhibition performance in CO_2 corrosion of N80 steel, *Corros. Sci*., 48(2006), p.3091.

[7] G.A. Zhang, M.X. Lu, C.W. Chai, and Y.S. Wu, Effect of HCO_3^- concentration on CO_2 corrosion in oil and gas fields, *J. Univ. Sci. Technol. Beijing*, 13(2006), No.1, p.44.

[8] C. Lin, X.G. Li, and C.F. Dong, Pitting and galvanic corrosion behavior of stainless steel with weld in wet-dry environment contaning Cl^-, *J. Univ. Sci. Technol. Beijing*, 14(2007), p.517.

[9] K. Videm, A. Dugstad, and L. Lunde, Parametric study of CO_2 corrosion of carbon steel, [in] *Corrosion Control in Petroleum Production*, Houston, 1994, p.14.

[10] T. Murata, E. Sato, and R. Matsuhashi, Factors controlling corrosion of steels in CO_2-saturated environments, [in] *Advances in CO_2 Corrosion*, Houston, 1984, p.64.

[11] Z.L. Pan, *Crystallography and Mineralogy* (in Chinese), Beijing Geology Press, Beijing, 1994, p.247.

[12] G. Schimit, CO_2 corrosion of steels: an attempt to range parameters and their effects, [in] *Advances in CO_2 Corrosion*, Houston, 1984, p.12.

[13] P. Sarin, V.L. Snoeyink, J. Bebee, W.M. Kriven, and J.A. Clement, Physico-chemical characteristics of corrosion scales in old iron pipes, *Water Res*., 35(2001), No.12, p.2961.

[14] A. Dugstad and L. Lunde, Influence of alloying elements upon the CO_2 corrosion rate of low alloyed carbon steels, *Corrosion*, 91(1991), p.473.